Angular momentum dependent absorption in ^{6}Li scattering

D. E. Trcka, A. D. Frawley, K. W. Kemper, D. Robson, J. D. Fox, and E. G. Myers
Department of Physics, Florida State University, Tallahassee, Florida 32306
(Received 1 November 1989)

Measurements are reported for (a) 50 MeV ^{6}Li+^{12}C elastic and inelastic scattering to the 2^+ (4.44 MeV), 0^+ (7.65 MeV), and 3^- (9.64 MeV) states in ^{12}C, (b) 20 MeV ^{6}Li+^{12}C elastic scattering, (c) 50 MeV ^{6}Li+^{16}O elastic and inelastic scattering to the unresolved $0^+/3^-$ (6.05/6.13 MeV) and $2^+/1^-$ (6.92/7.12 MeV) states in ^{16}O, and (d) 50 MeV ^{6}Li+^{9}Be elastic and inelastic scattering to the $\frac{5}{2}^-$ (2.43 MeV) state in ^{9}Be. Data were measured out to approximately $100^\circ_{\text{c.m.}}$. A mid-angle plateau characteristic of ^{6}Li scattering in the 5–10 MeV/nucleon energy range is confirmed in the ^{12}C and ^{16}O scattering but is not so apparent in the ^{9}Be scattering. Two energy-dependent, six-parameter optical model potentials, both of which describe ^{6}Li+^{12}C elastic scattering at ^{6}Li bombarding energies of 11, 20, 24, 30, 50, 60, 99, 156, and 210 MeV through the forward angle region before the plateau, are coupled with an angular momentum dependent imaginary potential. The results show improved descriptions of the plateau region and back angle scattering and a better description of 30 MeV ^{6}Li+^{12}C vector analyzing power data than has previously been published. The ^{6}Li+^{12}C inelastic scattering data are described by distorted-wave-Born-approximation calculations. Results of a double folded analysis of ^{6}Li+^{12}C elastic scattering at the above energies show a systematic variation of the double folded normalization, N, and the imaginary volume integral. ^{6}Li+^{16}O, ^{9}Be elastic scattering data are analyzed with optical model and double folded potentials and the inelastic scattering data are described with distorted-wave-Born-approximation calculations.

I. INTRODUCTION

More elastic scattering data exist over a wider range of energies and angles for ^{6}Li+^{12}C than for ^{6}Li scattering from any other target and perhaps any other heavy-ion target-projectile combination. This extensive body of data, including new data at 20 and 50 MeV reported here and 210-MeV data reported previously,[1] make it uniquely possible to study the energy dependence of the ^{6}Li+^{12}C nucleus-nucleus interaction. To date, it has not been possible to describe ^{6}Li+^{12}C elastic scattering with an optical potential whose parameters vary smoothly with energy.

Figure 1 shows elastic scattering data for ^{6}Li+^{12}C at 11 MeV,[2] 20 MeV (present work), 24 MeV,[3] 30 MeV,[3] 50 MeV (present work), 60 MeV,[4] 99 MeV,[5] 156 MeV,[6] and 210 MeV.[1] An examination of these data reveals that the elastic scattering of ^{6}Li from ^{12}C is characterized in the low-energy range (11 and 20 MeV) by a series of long period oscillations which extend throughout the measured angular distribution, and at high energies (99, 156, and 210 MeV) by a series of short period oscillations followed by a monotonic falloff in magnitude at larger angles. In the mid-energy range (24–60 Mev) the forward angle diffraction oscillations are followed by a plateau-like structure occurring in the angular region $60^\circ \leq \theta_{\text{c.m.}} \leq 90^\circ$ which is then followed by a rising back angle cross section. It is a common problem of energy-dependent optical potentials that they produce a deep minimum in the cross section at approximately $80^\circ_{\text{c.m.}}$ in this 10 MeV/nucleon energy range where, in fact, the plateau appears in the data.[2,7]

A similar but much more subtle plateau feature in ^{12}C+^{12}C scattering in the energy range of 5–10 MeV/nucleon has been described semiclassically by Brandan, Fricke, and McVoy[8,9] as originating from a transparency within the nuclear potential allowing the transmission of partial waves normally absorbed. Their analysis motivated the reintroduction of an angular momentum dependent imaginary potential into the present analysis of ^{6}Li+^{12}C scattering. This potential modification was introduced earlier to describe large angle α+^{40}Ca (Ref. 10) and ^{16}O+^{16}O scattering.[11] This present work examines the effect of coupling an energy-dependent optical potential which describes the data up to the region of the plateau with an angular momentum dependent absorption. The objectives are to see, first, if the description of the data in the plateau region and at the larger angles can be improved, and second, the effect upon the predicted vector analyzing power.

This work presents new experimental data for ^{6}Li+^{12}C elastic scattering at 20 MeV and for the elastic and inelastic scattering of ^{6}Li from ^{12}C, ^{16}O, and ^{9}Be at 50 MeV. Previous data for ^{6}Li+^{12}C elastic scattering at 50 MeV (Ref. 12) appeared to show evidence of the mid-angle plateau but were limited in scope. The purpose of the 50-MeV ^{6}Li scattering experiments reported here was to confirm the existence of the plateau at that energy for ^{12}C and to examine the scattering from ^{16}O and ^{9}Be for similar behavior. The 20-MeV ^{6}Li+^{12}C data were remeasured to check the normalization of previously published data,[13] since the magnitude of the existing forward angle data cannot be described with any systematic optical model parameters.

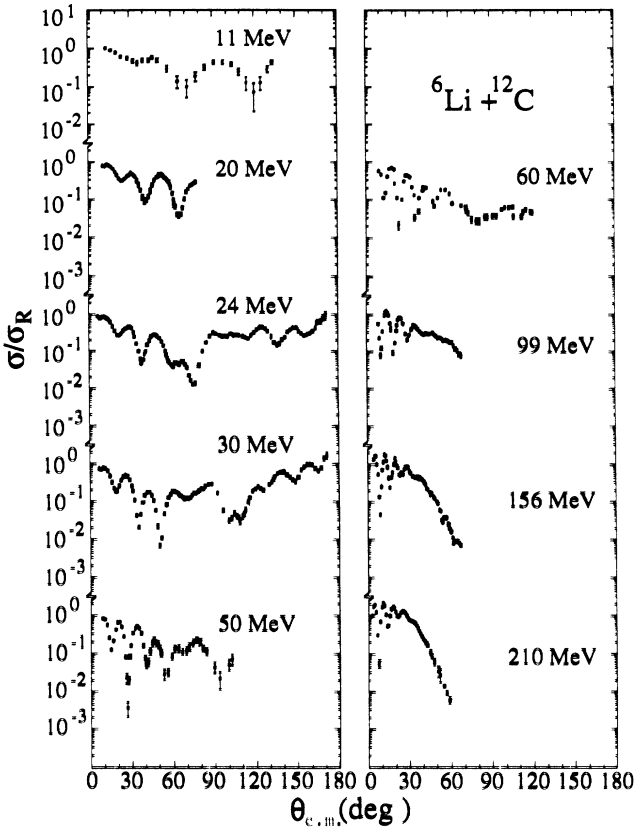

FIG. 1. Elastic scattering data for ^{6}Li+^{12}C at 11 MeV (Ref. 2), 20 MeV (present work), 24 MeV (Ref. 3), 30 MeV (Ref. 3), 50 MeV (present work), 60 MeV (Ref. 4), 99 MeV (Ref. 5), 156 MeV (Ref. 6), and 210 MeV (Ref. 1).

Section II discusses the experimental procedures and measurement of the ^{6}Li+^{12}C, ^{16}O, and ^{9}Be scattering data. Section III presents the analysis of the ^{12}C data and Sec. IV presents the analysis of the ^{16}O and ^{9}Be data.

II. EXPERIMENTAL PROCEDURES

The 50-MeV ^{6}Li beam used to obtain the scattering data reported here was produced with the Super FN tandem Van de Graaff coupled to the superconducting linear accelerator at Florida State University. A 76-cm-diam general purpose scattering chamber was used for the measurements. A wedge containing three silicon surface barrier E-ΔE telescopes spaced 7.5° apart was used for detecting the reaction products and a single, silicon surface-barrier detector fixed at 12° in the lab was used to monitor the target condition and charge integration. The detectors were collimated to subtend 0.6° in the lab, corresponding to 1.0° in the center of mass for ^{6}Li scattering from ^{9}Be, 0.9° for ^{12}C, and 0.8° for ^{16}O. The targets were 200 μg/cm^2 ^{12}C, 100 μg/cm^2 ^{9}Be, and 100 μg/cm^2 BeO. All of the targets were free standing

Differential cross-section measurements were taken over the angular range from 7° to approximately 75° in the lab, in 1°–2° steps. Standard electronics and computer codes were used for signal amplification and particle identification resulting in sorted linear energy spectra of the scattered ^{6}Li from the various targets.

Data were first taken for the ^{9}Be target because the measurements of both the elastic scattering and the inelastic scattering to the $5/2^-$ (2.43 MeV) state in ^{9}Be were necessary for the extraction of the ^{16}O yields from the BeO target at forward angles. In the spectra obtained with the BeO target, the peaks corresponding to the beryllium and oxygen ground states overlap at forward angles and the beryllium second-excited-state peak moves through the oxygen inelastic doublet peaks at larger angles. The measurements of the ^{9}Be cross sections then allowed the extraction of angular distribution data for ^{6}Li+^{16}O elastic and inelastic scattering to the unresolved $0^+/3^-$ (6.05/6.13 MeV) and $2^+/1^-$ (6.92/7.12 MeV) doublets. Because of the necessity of using the beryllium cross sections for the extraction of the oxygen yields, the beryllium data were measured three times to guarantee confidence and check the reliability of all the components in the measurement system. In the ^{12}C experiment, angular distribution data were measured for scattering to the ground state, and the 2^+ (4.44 MeV), 0^+ (7.65 MeV), and 3^- (9.64 MeV) excited states.

The measured differential cross sections were normalized to previously published angular distributions at 30 MeV for ^{6}Li+^{12}C,[7] 25.7 MeV for ^{6}Li+^{16}O,[7] and 32 MeV for ^{6}Li+^{9}Be.[14] The uncertainties due to statistics and yield determination are represented by the error bars in the data. The resulting absolute error in the normalization is less than 15% and consists of contributions from uncertainties in charge integration, target uniformity, deadtime determination, and the quoted absolute uncertainty of the previous normalizations.

The differential cross-section measurements for ^{6}Li+^{12}C elastic scattering at 20 MeV were made using the same chamber-detector-computer system, but only the super FN tandem Van de Graaff accelerator was used to accelerate the beam. The data were normalized to previously published data at 30 MeV.[7] The resulting normalization differs from that previously published[13] by a factor of 1.7.

III. ^{6}Li+^{12}C SCATTERING ANALYSIS

A. Energy dependence of the ^{6}Li+^{12}C optical potential

In the analysis presented in this section, the explicit nucleus-nucleus potential used was the standard Woods-Saxon optical potential

$$V(r)=-f(r)(V+iW)+V_c(r) \tag{1}$$

with the Woods-Saxon form factor given by

$$f(r)=\left[1+\exp\left[\frac{r-R}{a}\right]\right]^{-1} \tag{2}$$

and the Coulomb potential given by

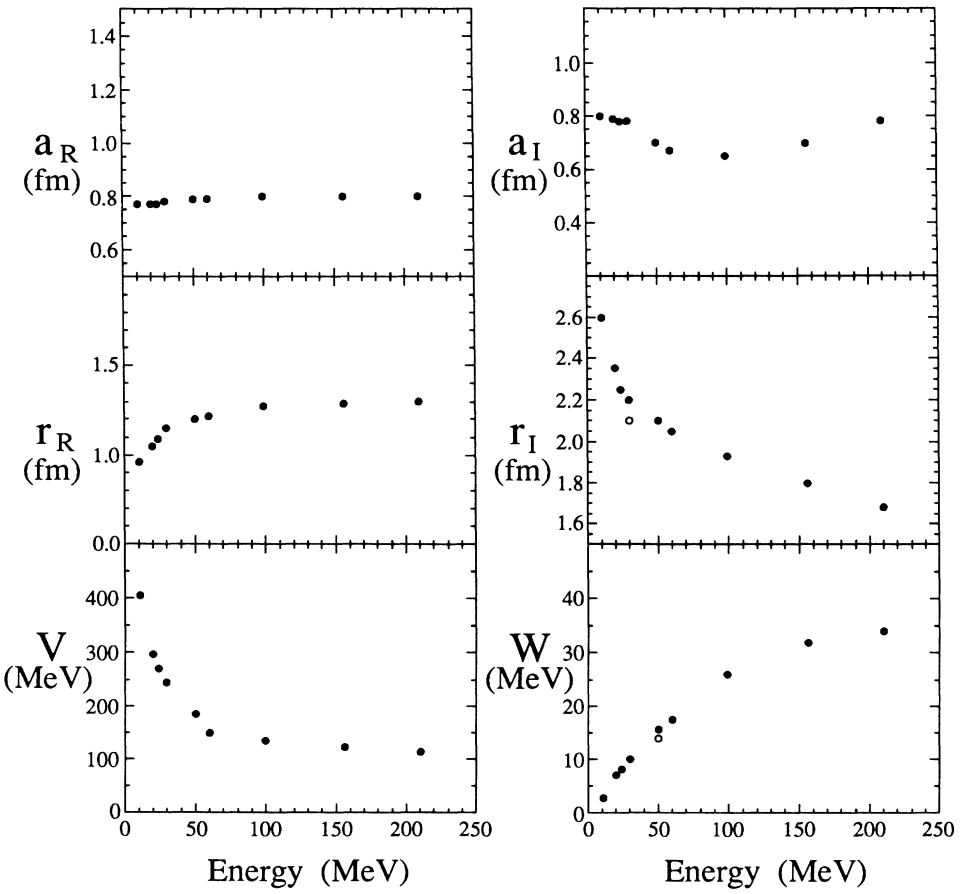

FIG. 2. Behavior of the optical potential parameters versus energy for the OM1 potentials. (Open circles represent alternate values used for the OM2 potential.)

$$V_c(r)=\frac{Z_1Z_2e^2}{2R_c}\left[3-\frac{r^2}{R_c^2}\right], \quad r\le R_c$$
$$=\frac{Z_1Z_2e^2}{r}, \quad r>R_c \ . \tag{3}$$

Standard notation is used throughout, where V, R_R, and a_R are the strength, radius, and diffuseness of the real potential and W, R_i, and a_i denote the strength, radius, and diffuseness of the imaginary potential. The interaction radii are defined by

$$R_x=r_x A_T^{1/3} \ , \tag{4}$$

where r_x is the radius parameter and A_T is the target mass. When a spin-orbit potential was used in the calculations, it had the form

$$V^{LS}(r)=\left[\frac{\hbar}{m_\pi c}\right]^2\frac{V_{SO}}{r}\frac{d}{dr}\{1+\exp[(r-R_{SO})/a_{SO}]\}^{-1}$$

with $V_{SO}=1.3$ MeV, $r_{SO}=1.1$ fm, and $a_{SO}=0.37$ fm. The Coulomb radius parameter, r_c, was fixed at 2.3 fm for all the calculations since it corresponds to the combined radii of ^{6}Li and ^{12}C as deduced from electron scattering. The variation in the cross section due to changes in this parameter is known to be small.[15] The optical model code[16] HERMES was used for the calculations.

Two energy-dependent potentials, labeled OM1 and OM2, are presented here for comparison. Both sets use essentially the same energy-dependent imaginary potential parameters, but the behavior with energy of their real potential parameters differs significantly. In the OM1 potentials the strength of the real part varies roughly hyperbolically from 405 MeV (at $E_{Li}=11$ MeV) to 113 MeV (at $E_{Li}=210$ MeV) and the real radius and diffuseness vary smoothly, but not linearly, through the range 0.96–1.3 fm and 0.77–0.80 fm, respectively. The real and imaginary parameters for the OM1 potential are plotted versus energy in Fig. 2.

In the OM2 potentials the strength of the real part varies linearly from 244 MeV (at $E_{Li}=11$ MeV) to 205 MeV (at $E_{Li}=210$ MeV) and the real radius and diffuseness remain fixed at 1.18 and 0.74 fm, respectively. The imaginary potential parameters used for OM2 are the same as those for OM1, with two exceptions. At 30 MeV, a value of 2.1 fm was used for r_I and at 50 MeV a value of 14.0 MeV was used for the imaginary strength. These two alternate values for the OM2 imaginary parameters are shown by the open circles in Fig. 2. The

TABLE I. ^{6}Li + ^{12}C potential parameters.

E_{Li} (MeV)	Potential	V (MeV)	N	r_R[a] (fm)	a_R (fm)	W (MeV)	r_I[a] (fm)	a_I (fm)	$J_c/\Delta J$
11	OM1	405.0		0.96	0.77	2.70	2.60	0.80	
	OM2	244.0		1.18	0.74	2.70	2.60	0.80	
	DF		0.72			2.19	2.90	0.57	
20	OM1	285.0		1.05	0.77	7.00	2.35	0.79	
	OM2	242.2		1.18	0.74	7.00	2.35	0.79	
	DF		0.73			10.78	1.63	1.04	
24	OM1	270.0		1.09	0.77	8.00	2.25	0.78	12.0/2.0
	OM2	241.3		1.18	0.74	8.00	2.25	0.78	12.0/2.0
	DF		0.73			13.20	1.52	0.90	
30	OM1	244.0		1.15	0.78	10.00	2.20	0.78	12.5/2.0
	OM2	240.3		1.18	0.74	10.00	2.10	0.78	
	DF		0.69			8.65	2.10	0.82	
50	OM1	185.0		1.20	0.79	15.50	2.10	0.70	15.0/2.0
	OM2	236.4		1.18	0.74	14.00	2.10	0.70	
	DF		0.66			12.00	2.20	0.68	
	OM1~	173.9		1.18	0.84	13.00	2.27	0.55	
	OM1J~[b]	167.1		1.20	0.79	13.14	2.19	0.88	15.0/2.0
60	OM1	150.0		1.22	0.79	17.50	2.05	0.67	
	OM2	234.4		1.18	0.74	17.50	2.05	0.67	17.5/2.0
	OM2J[b]	234.4		1.18	0.74	21.50	1.72	0.91	17.5/2.0
	DF		0.62			25.90	1.72	0.91	
	OM2~	179.4		1.41	0.66	44.90	1.25	1.06	
	OM2J~[b]	231.7		1.16	0.73	70.65	0.71	1.33	18.0/2.0
99	OM1	135.0		1.27	0.80	26.00	1.93	0.65	
	OM2	225.8		1.18	0.74	26.00	1.93	0.65	
	DF		0.61			43.70	1.50	0.89	
156	OM1	123.0		1.29	0.80	32.00	1.80	0.70	
	OM2	215.0		1.18	0.74	32.00	1.80	0.70	
	DF		0.60			44.38	1.82	0.56	
210	OM1	113.0		1.30	0.80	34.00	1.68	0.78	
	OM2	205.0		1.18	0.74	34.00	1.68	0.78	
	DF		0.57			59.10	1.31	0.90	

[a] $R_x = r_x A_T^{1/3}$.

[b] The character "J" included in the potential name denotes the use of J-dependent absorption with the indicated values for J_c and ΔJ.

values of the parameters for the OM1 and OM2 potentials are contained in Table I.

The OM1 potentials were constructed by surveying previously cataloged[17] potentials. When the energy dependence of the parameters of these potentials is examined, trends appear evident, but there remain discontinuities. However, these potentials were the result of the parameter searching required to fit the entire measured angular range of data. If only the portion of the data in the forward angles is considered, i.e., the data forward of the plateau, the discontinuous or ill-behaved parameters could be brought back to the trend line and the description of the data up to the plateau region remained good. In this manner, the OM1 potentials were constructed without the use of the χ^2 parameter optimization codes. The decrease in the real potential, as the bombarding energy is increased, found in the present work is similar to that found by Nadasen *et al.*[1]

The real part of the OM2 potential was constructed to represent a simple potential whose real strength is approximately six times the nucleon-nucleus potential and which varies by 10% from 11 to 210 MeV.

Figure 3 contains a comparison of the calculated differential cross sections with the measured data from 11 to 210 MeV. Both the OM1 and OM2 potentials fit the forward angle cross-section data through approximately 60°$_{c.m.}$ at all energies (except for the 99-MeV data where the agreement is good only through approximately 30°). Both potentials predict similar behavior at the lower energies (11, 20, and 24 MeV) although they differ in some details. The OM1 potentials describe the data in the high-energy range (156 and 210 MeV) better than the OM2 potentials, while the OM2 potentials describe the data in the mid-energy range (30, 50, 60, and 99 MeV) better than the OM1 set.

The 20-MeV data shown in Fig. 3 were measured in order to extend previous measurements[13] to more forward angles and to check normalization. As stated earlier, the previous data had to be multiplied by 1.7. The renormalized 20-MeV data are in good agreement with the forward angle calculations in the first oscillation, but the magnitude of the calculations are significantly lower than

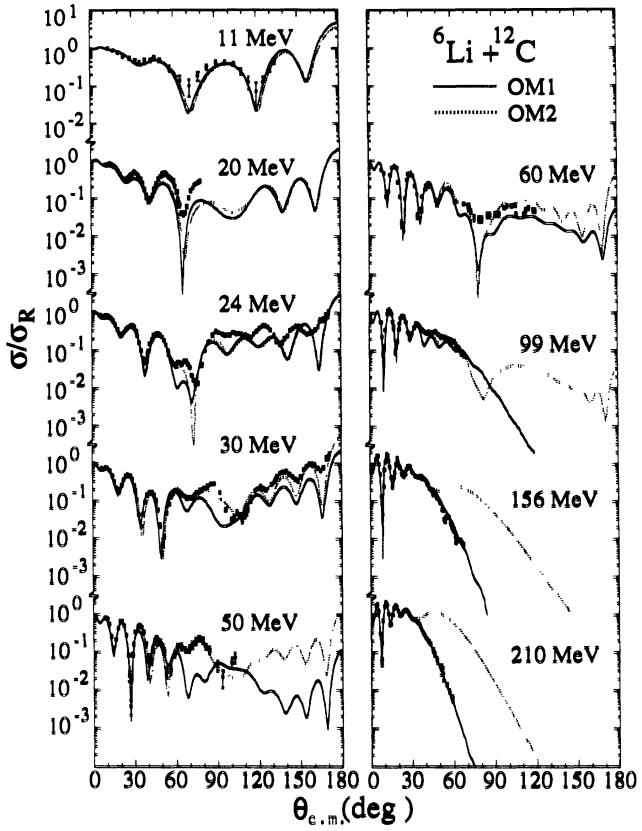

FIG. 3. Optical model descriptions of ^{6}Li+^{12}C elastic scattering data using the OM1 and OM2 potentials.

the magnitude of the data in the second and third oscillations. This may be due to a resonance known to be present in this energy region.[18]

The normalization of the original 99-MeV data[5] remains in question. A previous study[7] of the energy dependence of the optical potentials found it necessary to rescale the original data[5] to allow a meaningful analysis. In the present work, the original data have been normalized to the forward angle calculations. The resulting description of the data is good through the first four oscillations, but then the calculations show more structure than appears in the data. While it could be argued that the inclusion of these data in a study of energy-dependent potentials is inappropriate, it is felt that the gap in energy between 60 and 156 MeV would be too large without including it.

By employing the χ^2 parameter optimization routines it is possible to improve the description of these data at any particular energy. However, such searches lead to parameter sets which have little, if any, systematic behavior with energy and thus little predictive value. It has been shown here that a potential with systematic parameters can describe the elastic scattering data well through the forward angle oscillation region over a wide energy range. To improve the description beyond this, one must employ searching in combination with more exotic potential models. The following section examines the effect of complementing the energy-dependent potential with angular momentum dependent absorption in order to see if the back angle description can be improved.

B. The effect of an angular momentum dependent imaginary potential

Angular momentum dependent absorption was first introduced to successfully describe ^{16}O+^{40}Ca, ^{16}O+^{16}O, and α+^{40}Ca scattering.[10,11,19–21] The justification for including a J dependence in the absorptive potential is based on the conservation of angular momentum and energy in the various reaction channels. The incident heavy ions may carry a greater angular momentum into the scattering region than any of the reaction channels can carry away. For these angular momenta the elastic wave will not be attenuated, even in the interior of the nuclear interaction because the elastic channel and the reaction channels are poorly matched.[19] The motivation to introduce additional parameters via J-dependent absorption stems from the difficulties regarding optical model analysis of ^{6}Li scattering. ^{6}Li scattering data show unusually large cross sections at backward scattering angles (at intermediate energies) and have the mid-angle plateau which can be fitted in a conventional optical model only by the use of parameters which do not vary smoothly with energy. Further, vector analyzing power data are difficult to explain using just a spin-orbit term and are sensitive to coupled channels effects.[22–24] Large backward angle cross sections for ^{6}Li are reminiscent of similar effects observed with light ions scattered by light targets which could be described by using angular momentum dependent absorption.[10]

In the present study the availability of polarized ^{6}Li data is of interest because J-dependent absorption yields polarization effects. This arises because the conserved quantity is the total angular momentum, J, and each orbital angular momentum L is coupled to three J values, i.e., $J=L,L\pm1$ and each of these amplitudes will be different due to the assumed absorption dependence on J. Polarization arises from the differences between these three contributions as it does with a conventional spin-orbit interaction. However, the use of J dependence in the absorptive potential corresponds to modeling effects which arise from the coupling to all nonelastic exit channels taken together, rather than attempting to solve the explicit channel coupling problem.[23]

In order to have different absorption for different partial waves, the standard Woods-Saxon absorptive term in the optical potential, $W(r)$, is modified in the code HERMES by the addition of an angular momentum dependent form factor, $f(J)$. Thus, the imaginary potential becomes $f(J)W(r)$

$$W(r)\rightarrow f(J)W(r)\ , \tag{5}$$

where $f(J)$ is given by

$$f(J)=\left[1+\exp\left[\frac{J-J_c}{\Delta J}\right]\right]^{-1} \tag{6}$$

in which J_c is the angular momentum cutoff parameter and ΔJ is the angular momentum cutoff diffuseness pa-

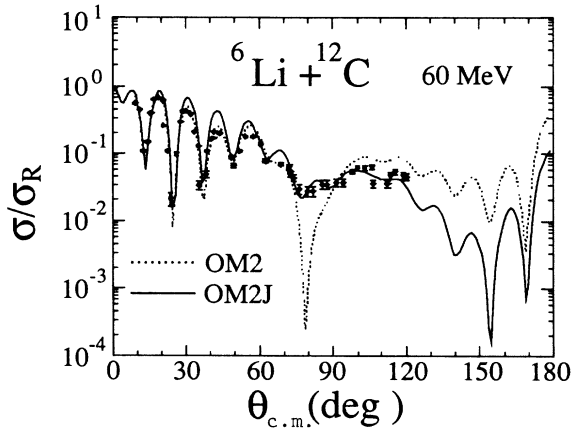

FIG. 4. Comparison of optical model descriptions of 60-MeV ^{6}Li+^{12}C elastic scattering with (OM2J) and without (OM2) J dependence.

rameter. Using very large values of J_c, well beyond L_{gr}, the grazing angular momentum given by

$$L_{gr} \approx kR \approx 1.4k(A_T^{1/3} + A_P^{1/3}) , \quad (7)$$

where k is the wave number of the projectile, produces no effect in the scattering calculations. As J_c moves into the approximate range of L_{gr} the back angle cross section begins to show an increase in magnitude. The lower the value of J_c, i.e., the stronger the J-dependent absorption, the more pronounced this effect becomes. Very small values of ΔJ create a sharp edge in the absorption potential and result in the typical black disk scattering pattern of diffraction oscillations extending to large angles. Very large values result in cross sections identical to those predicted from the standard Woods-Saxon imaginary term.

In the 60-MeV OM1 and OM2 calculations there appears the previously mentioned dip in the angular distributions at approximately 80°$_{c.m.}$ where the data have, in fact, a plateau (see Fig. 3). In order to see if the description in this region could be improved and the dip eliminated, strong J dependence was used with the OM2 potential for the calculations at 60 MeV (OM2J). The result is shown together with the calculations without J dependence (OM2) in Fig. 4 and shows that J dependence is able to remove the dip in the calculations when accompanied by an increase in the strength of the imaginary potential.

Reviewing the data and calculations of Fig. 3, in the low-energy (11 and 20 MeV) and high-energy (156, 210) ranges there is no compelling need for modifications to the energy-dependent potential, as the OM1 potential describes the measured data (except for the previously discussed 20-MeV data). At 24 MeV the calculations are low in the 90°$_{c.m.}$ – 180°$_{c.m.}$ range and the oscillations are out of phase with the data. Figure 5 shows a comparison of these data with J-dependent calculations using the OM1 and OM2 potentials where J dependence was employed and no changes were made in other parameters. The effects are to enhance the mid- and back angle magnitudes, more at the top of the oscillations than in the dips, and to shift the phase slightly in the mid-angle region. The result is that the magnitude of the cross section more nearly matches that of the data, but the shape and phase of the oscillations remain poorly described. Stronger J dependence, i.e., a lower value of J_c, will increase the back angle enhancement, which may be balanced or tempered by increasing W, but does not change the basic shape or phase of the oscillations in the back angles.

An analysis of the 30-MeV data allows a more critical examination of the role of J dependence in ^{6}Li scattering because not only do there exist high-quality elastic scattering data, but also vector analyzing power (VAP) data. Figure 6 shows a comparison of the elastic scatter-

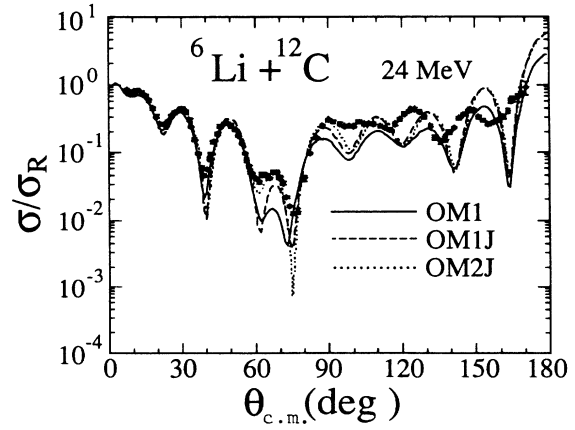

FIG. 5. Optical model descriptions of 24-MeV ^{6}Li+^{12}C using the OM1 potential and the OM1 and OM2 potentials with J dependence (OM1J and OM2J).

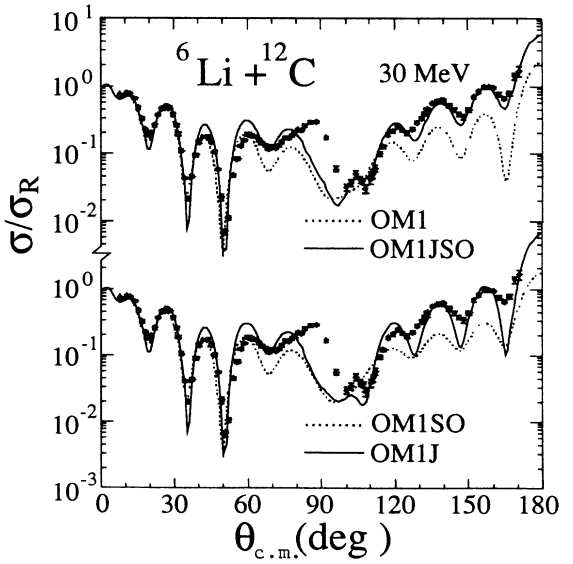

FIG. 6. Optical model descriptions of 30-MeV ^{6}Li+^{12}C using the OM1 potential without J dependence or a spin-orbit interaction (OM1), with a spin-orbit interaction (OM1SO), with J dependence (OM1J), and with both spin orbit and J dependence (OM1JSO).

ing cross sections with four calculations employing (1) the OM1 potential, (2) the OM1 potential with J dependence (OM1J), (3) the OM1 potential with a weak spin-orbit potential (OM1SO), and (4) the OM1 potential with J dependence and a spin-orbit potential (OM1JSO). The magnitude of the OM1 potential calculations is less than the magnitude of the back angle scattering data although the phase match between the back angle data and the calculations is good. The addition of J dependence (OM1J), without changing any optical parameters enhances the back angle magnitude so that it more nearly matches that of the data although the dips are still too deep. Using the spin-orbit potential and no J dependence (OM1SO) has the effect of slightly dampening the back angle oscillations, and the combination of both the spin orbit and J dependence (OM1JSO), without any reoptimization of optical parameters, produces the desirable effect of increasing the back angle magnitude and filling in the minima yielding a better fit throughout than previously obtained with optical model, double folding, or coupled-channels calculations.[3] These same results are seen with the OM2 potential.

A comparison of the VAP measurements with the calculations using the OM1J, OM1SO, and OM1JSO potentials is presented in Fig. 7. An examination of the forward angles (where the measurements exist) shows that the J-dependent calculation (OM1J) describes the data as well, or better than, previously published calculations.[22] The spin-orbit potential (OM1SO) pulls down the calculations in the region following both the sharp negative and positive spike whereas the data are unmistakably higher. The combination of both spin orbit and J dependence produces an acceptable fit, which is consistent with the description of the elastic scattering data.

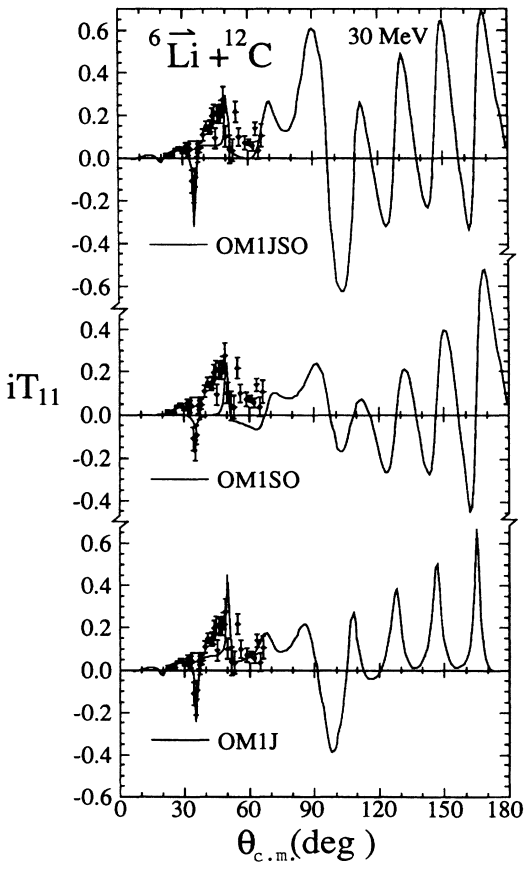

FIG. 7. Optical model descriptions of the 30-MeV ^{6}Li+^{12}C vector analyzing power using the OM1 potential with J dependence (OM1J), with a spin-orbit interaction (OM1SO), and with both J dependence and a spin-orbit interaction (OM1JSO).

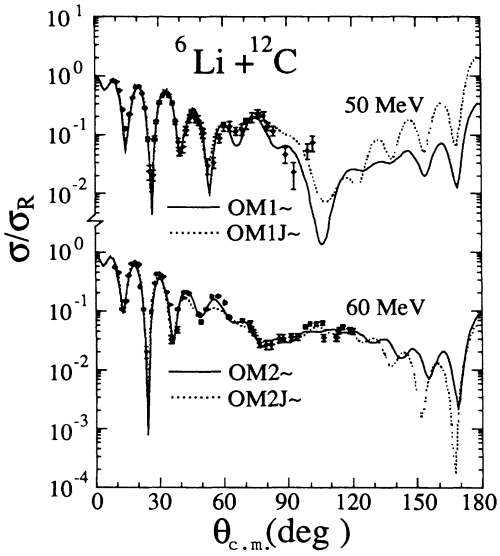

FIG. 8. Optical model descriptions of 50- and 60-MeV ^{6}Li+^{12}C elastic scattering resulting from a six-parameter search using the OM1 and OM2 potentials for starting values both with J dependence (OM1$J^{\sim}$, OM2$J^{\sim}$) and without J dependence (OM1$^{\sim}$, OM2$^{\sim}$).

Thus, while J-dependent absorption alone improves the elastic scattering description and produces a VAP that is in good agreement with the VAP data, there is evidence that a model involving both J-dependent absorption and a spin-orbit interaction could be most useful. It is with back angle VAP measurements that this question could best be examined further. The calculations shown in Fig. 7 indicate that in the $120^{\circ}_{c.m.}-150^{\circ}_{c.m.}$ region the inclusion of the weak spin-orbit interaction, with or without J dependence, results in deep negative dips in the VAP whereas the calculations involving J dependence alone remain positive. VAP measurements in this angular region could provide evidence regarding the role of both the spin-orbit interaction and J-dependent absorption in ^{6}Li scattering.

Parameter optimization using χ^2 search routines, with and without the inclusion of J dependence, yield good descriptions of the 50-MeV (OM1~, OM1J~) and 60-MeV (OM2~,OM2J~) data (Fig. 8). However, without back angle data and VAP data there are no meaningful criteria to evaluate the role of J dependence in the scattering process.

C. Double folding analysis

The ^{6}Li+^{12}C elastic scattering data were analyzed again using the double folding (DF) model for construct-

ing the real part of the optical potential.[25,26] This model derives the real potential by integrating an effective microscopic nucleon-nucleon interaction over the target and projectile matter densities. The real optical potential is given by

$$V(\mathbf{R})=N\int d\mathbf{r}_a\int d\mathbf{r}_A\rho_a(\mathbf{r}_a)\rho_A(\mathbf{r}_A)V(\mathbf{s}=\mathbf{r}_a-\mathbf{r}_A+\mathbf{R}) , \tag{8}$$

where ρ_a and ρ_A are the density distributions of the projectile and target nuclei, V is the effective nucleon-nucleon interaction, and N is the overall potential normalization factor. While the integration is over mass densities and not nucleons, the coordinates may be visualized by considering the coordinate $\mathbf{R}$ as the vector from the center of mass of the target nucleus to the center of mass of the projectile nucleus, $\mathbf{r}_a$ as the vector from the center of mass of the projectile nucleus to a projectile nucleon, $\mathbf{r}_A$ as the vector from the center of mass of the target nucleus to a target nucleon, and $\mathbf{s}$ as the vector from the target nucleon to the projectile nucleon specified by $\mathbf{r}_a$ and $\mathbf{r}_A$ ($\mathbf{s}=\mathbf{r}_a-\mathbf{r}_A+\mathbf{R}$). The effective interaction used is the $M3Y$ ($S=T=0$) interaction of Bertsch *et al.*[27] given by

$$V_{00}(s)=7999\frac{e^{-4s}}{4s}-2134\frac{e^{-2.5s}}{2.5s}-390\delta(s) , \tag{9}$$

where the single-nucleon knockout exchange[28–30] (SNKE) delta term is included to account for antisymmetrization of the total wave function, at least in the tail region of the interaction, and allow for the exchange of nucleons in the scattering process.

The ^{6}Li density used was that of Suelzle *et al.*[31] obtained from the charge density determined by electron scattering, with the finite size of the charge distribution of the proton unfolded. A harmonic-oscillator density was used for the ^{12}C density.[3] For the J-dependent DF calculations the form of the imaginary potential term was modified to include a J-dependent multiplicative factor in the same manner as described earlier.

The ^{6}Li+^{12}C data were analyzed with the DF real and Woods-Saxon imaginary potential in which the normalization of the real DF potential and the three variables of the imaginary potential were varied to obtain the optimum fit to the data. The resulting parameters (DF) are contained in Table I.

The double folded potentials, combined with the standard Woods-Saxon imaginary potential, describe the data with varying degrees of success. They appear to suffer the same problem as the energy-dependent Woods-Saxon optical potential in that they are able to describe the cross sections in the low- and high-energy ranges, but do not do as well in the mid-energy region. At 11, 156, and 210 MeV the description of the data is exemplary, but at 20, 30, 50, and 60 MeV the descriptions mimic the cross sections but miss some of the details. The calculations for 50 and 210 MeV are shown in Fig. 9 and the behavior of the DF normalization and imaginary volume integral

$$J_W=\tfrac{4}{3}\pi WR_I^3[1+(\pi a_I/R_I)^2]$$

with energy are shown in Fig. 10. As seen in Fig. 9, the double folded potential describes the data forward of the plateau, but is unable to fit the details of the plateau region. The calculations show that the SNKE contribution in ^{6}Li scattering does not have the predicted energy dependence.[32] Using the predicted energy-dependent values for the SNKE strength worsens the description of the data at all energies. It was found that a constant value of -390 MeV for the SNKE strength best described the elastic cross sections throughout the energy range under examination. The present analysis is the first double folded analysis of the 210-MeV ^{6}Li+^{12}C elastic scattering and the results yield a value of 0.57 for the normalization of the double folded potential. The strength of the absorption as evidenced by the imaginary strength

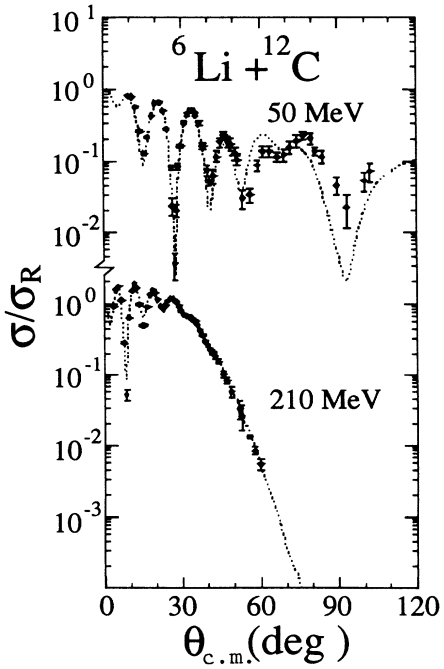

FIG. 9. Double folded potential descriptions of 50- and 210-MeV ^{6}Li+^{12}C elastic scattering.

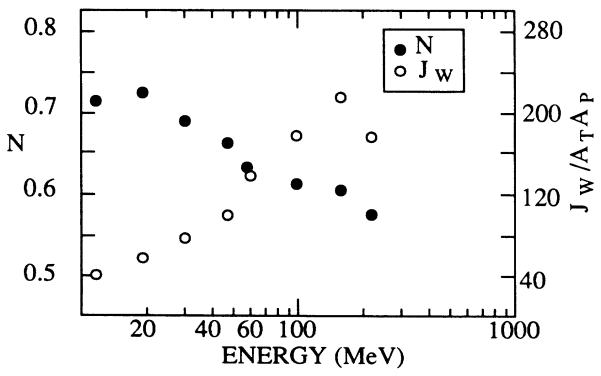

FIG. 10. Behavior versus energy of the double folded normalization N and the imaginary volume integral per nucleon J_W/A_TA_P for ^{6}Li+^{12}C from 11 to 210 MeV.

of the optical potentials OM1 and OM2 suggests that the ΔU contribution to the effective interaction,[25] i.e., that arising from coupling to inelastic states, is non-negligible. Since double folding does not model the real part of this contribution[25,26] it should not be surprising that the double folding description of the data is less than satisfactory.

D. ^{6}Li+^{12}C inelastic scattering analysis

The inelastic scattering analyses were conducted using the distorted-wave-Born-approximation (DWBA) code DWUCK4 (Ref. 33) in which the 50-MeV ^{12}C potential, OM1 in Table I, was employed for calculating the initial and final distorted waves. A macroscopic collective-model transition form factor was used in which the transition potential is the derivative of the complex optical potential and the nuclear radius is described by a multipole expansion employing β as the deformation parameter. The resulting calculated cross section scales as β^2 and the value of β was extracted by normalizing the calculations to the data.

For the examination of J-dependent inelastic scattering, DWUCK4 was modified in the same manner as described previously for the code HERMES. Here this modification provides only a poor approximation to rigorous angular momentum dependence, for no attempt was made to modify the code to account for the spin of both the ejectile and residual particles and the change in J_c in the exit channel. The $\mathbf{J}_{tot}$ of the system is constructed from the spin of the projectile, i.e., $\mathbf{J}_{tot}=\mathbf{L}+1$ and

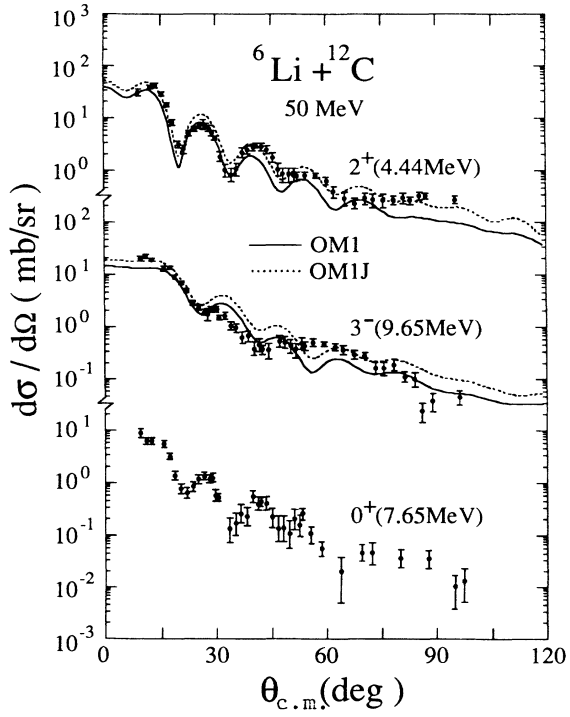

FIG. 11. Data and DWBA calculations for ^{6}Li+^{12}C scattering to the 2^+ (4.44 MeV), 0^+ (7.65 MeV, data only), and 3^- (9.64 MeV) states in ^{12}C.

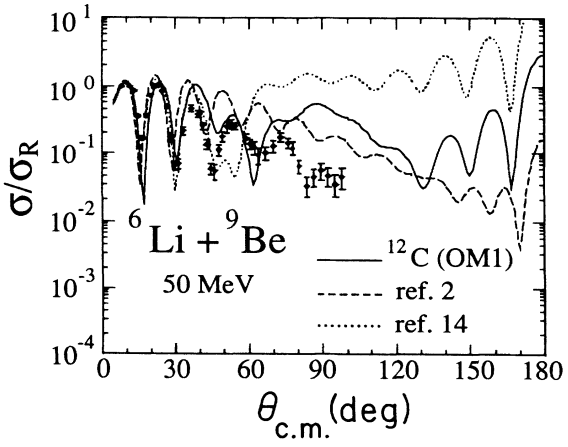

FIG. 12. Comparison of 50-MeV ^{6}Li+^{9}Be elastic scattering with optical model calculations using the OM1 potentials (Table I), Refs. 2 and 14 (Table III).

used in both the entrance and exit channel distorted-wave calculations.

Figure 11 shows the calculations and experimental data for scattering to the 4.43 (2^+), 7.65 (0^+), and 9.64 (3^-) MeV states in ^{12}C. These data do not appear to show any evidence of the plateau structure observed in the elastic scattering. The dashed and solid lines present the results of the calculations with J dependence (OM1J) and without J dependence (OM1), respectively, for scattering to the 2^+ and 3^- states. Since this transition potential is inadequate to describe monopole and dipole transitions,[34,35] the calculations for the 0^+ state have been omitted. In both cases it can be seen that the effect of the J dependence does not change the basic shape or character of the inelastic calculations, but rather, it increases the magnitude of the predicted cross section, showing a slightly greater enhancement at the back angles.

The calculations for the 4.43-MeV 2^+ state are in good agreement with the data. It was found here, as in very

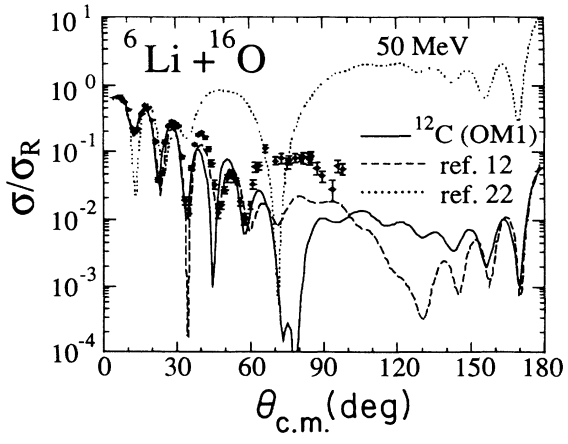

FIG. 13. Comparison of 50-MeV ^{6}Li+^{16}O elastic scattering with optical model calculations using the OM1 potentials (Table I), Refs. 12 and 22 (Table II).

early studies[36] of inelastic ^{6}Li scattering, that the imaginary transition strength accounts for the majority of the inelastic strength. The value of $\beta R_I = 1.40$ fm is in excellent agreement with the value of 1.48 fm for 30-MeV scattering.[3] In the case of the calculations for the 9.64-MeV 3^- state, the experimental data show less structure than the calculations. The value of βR_I for the 9.64 state is 1.40 fm compared with 1.91 fm previously reported for 30-MeV scattering.[3]

IV. ^{6}Li+^{9}Be, ^{16}O SCATTERING ANALYSIS

The 50-MeV elastic scattering cross sections for ^{9}Be and ^{16}O are shown in Figs. 12 and 13, respectively. The ^{16}O data display the mid-angle plateau characteristic of ^{6}Li+^{12}C scattering seen in the previous section, while in the ^{9}Be data this feature is not as apparent. The ^{9}Be angular distribution data proceed through a series of Fraunhofer oscillations of descending magnitude out to approximately 100° in the center of mass with little evidence of a plateau.

For the analyses of these data it is first important to recognize that since there does not exist an extensive body of elastic scattering data over a wide rangle of energies for ^{6}Li+^{9}Be, ^{16}O as there is for ^{6}Li+^{12}C, it is not possible to attempt an energy-dependent analysis. Such an analysis would, if possible, provide potentials able to describe the behavior of the data in the forward angle diffraction region as a function of energy and provide an energy-dependent potential which could be coupled with the J-dependent imaginary potential to attempt to improve the fit to larger angle data. Further, the crucial VAP data do not exist. Thus, the addition of the J dependence becomes meaningless, for, as shown in the ^{12}C analysis and as will be shown in the ^{9}Be and ^{16}O analysis, the optical potential is versatile enough to fit the elastic scattering data at a given energy.

In order to investigate the sensitivity of the angular distribution to the details of the potential, the ^{9}Be and ^{16}O data are compared with three different prescriptions provided by three different optical potential sets. Figures 12 and 13 show these calculations compared with the 50-MeV data for ^{9}Be and ^{16}O, respectively. The ^{9}Be data are compared with predictions using potentials from (1) the 50-MeV ^{12}C study reported here (the OM1 potential, Table I), (2) the energy-dependent potential of Ref. 14, and (3) the energy-dependent potential of Poling *et al.*[2] The ^{16}O data are compared with predictions using potentials from (1) Van Verst *et al.*,[22] (2) Chua *et al.*,[12] and (3) the 50-MeV ^{12}C study reported here (the OM1 potential, Table I). While the calculations for the different potentials predict markedly different angular distributions, they are remarkably consistent in the description of the forward angles containing the first oscillation. This is evidence, albeit not unsuspected,[37] that the far forward angle scattering is not sensitive to the details of the shape of the nuclear potential, and that the scattering is dominated by the Coulomb potential. Calculations show that the strength of the real nuclear potentials in the region around 7 fm is on the order of $\frac{1}{100}$ of the Coulomb potential. Further, absorption is small at these scattering angles, so the details of the imaginary part of the potential are not determined by the scattering. Thus, the particular value of the strength, radius, and diffuseness of the nuclear optical potential is not critical to the prediction of the far forward angle elastic scattering.

The starting point for the Woods-Saxon optical model analysis of the ^{16}O elastic scattering data was the potential of Chua *et al.*[12] This earlier study only reported data for the forward angle oscillatory region and the derived potential does not really provide a good description of the more detailed data reported here. The six potential parameters were varied to obtain the best description of the data and the result is shown in Fig. 14. The resulting parameters (OM) are contained in Table II and the resulting description of the data is good.

The ^{6}Li+^{16}O elastic scattering data were also analyzed with the double folded real potential in the manner of the ^{12}C analysis in Sec. III. The ^{6}Li density was that of Suelzle[31] and a harmonic-oscillator density was used for the ^{16}O target nuclei.[7] The normalization N and the three imaginary parameters of the Woods-Saxon imaginary potential were varied to obtain the optimum fit. The results are shown in Fig. 14. The resulting DF description is quite good through the dip preceding the plateau at approximately 55°, but the calculation is unable to describe the plateau. The resulting parameters are contained in Table II.

The starting point for the optical model analysis of the ^{6}Li+^{9}Be elastic scattering data was the potential of Ref. 14. Again, the six potential parameters were varied to obtain the optimum fit to the data. The result (the OM potential, Table III) is shown in Fig. 15 which shows that in the forward angle diffraction region and in the region of the two oscillations at larger angles, the data are described well. Between these two regions there is a sharp minimum in the calculations that does not describe the data. But aside from this weakness, the potential presents a good description considering that the ^{6}Li+^{9}Be elastic scattering involves strong coupled-channels effects which would be expected to make optical potential analysis difficult. First, the breakup effects of both ^{6}Li and ^{9}Be must play an important role in the absorption,[23]

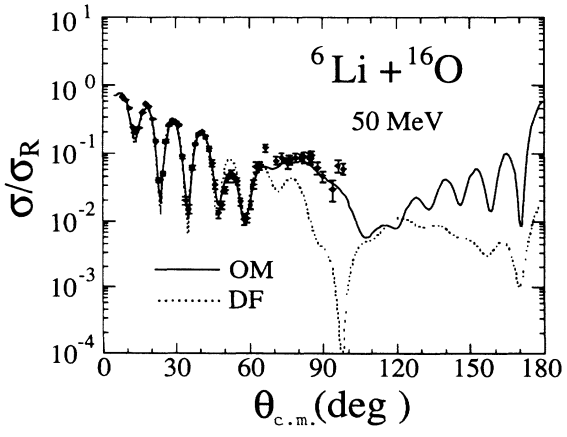

FIG. 14. Optical model (OM) and double folded (DF) descriptions of 50-MeV ^{6}Li+^{16}O elastic scattering.

TABLE II. ^{6}Li+^{16}O 50-MeV potential parameters.

Potential	V (MeV)	N	r_R[a] (fm)	a_R (fm)	W (MeV)	r_I[a] (fm)	a_I (fm)
Ref. 12	210.0		1.30	0.70	25.00	1.70	0.90
Ref. 22	124.8		1.15	0.91	7.33[b]	1.79	0.82
OM	185.6		1.37	0.70	16.97	1.88	0.82
DF		0.65			14.76	2.13	0.50

[a]$R_x = r_x A_T^{1/3}$.
[b]Strength of a surface derivative imaginary potential.

second, both the 2.43-MeV state in ^{9}Be and the 2.18-MeV state in ^{6}Li are easily excited and are certainly strongly coupled to the elastic scattering, and third, the quadrupole reorientation of the ^{9}Be ground state has been shown to play a significant role in elastic scattering.[38]

The results of the DF analysis of the ^{6}Li+^{9}Be elastic scattering data are shown in Fig. 15. The most obvious difference between these predictions and the optical potential predictions is in the cross section at the back angles. The DF calculations fit the measured data fairly well and then falloff precipitously, whereas the optical potential calculations using the OM potential, show a rising back angle cross section.

The inelastic scattering of ^{6}Li to the $5/2^-$, 2.43-MeV state in ^{9}Be and the $0^+/3^-$ doublet (6.05 and 6.13 MeV) and the $2^+/1^-$ doublet (6.92 and 7.12 MeV) in ^{16}O was analyzed in the same manner as the ^{12}C analysis. The potential labeled OM was used in both the ^{9}Be and ^{16}O initial and final distorted-wave calculations, without J dependence, and the transition potential was complex, constructed from the derivative of the distorted-wave potential.

The measured cross-section data for the scattering to the $0^+/3^-$ doublet in ^{16}O are compared in Fig. 16 with the calculated contribution from the 3^- transition. It is evident from this comparison that the major contribution is from the 3^- transition. The value of βR_I of 1.50 fm for the 3^- transition compares with 1.55 fm previously determined for 30-MeV scattering.[7] Also shown in Fig. 15 are the data for the scattering to the $2^+/1^-$ doublet in ^{16}O compared with the calculations for the contribution from the 2^+ transition. The calculations are scaled to $\beta R_I = 0.73$ determined from (p,p') studies.[34] Since the derivative form of the transition potential is inadequate to describe monopole and dipole transitions,[34,35] only the calculations for the 3^- and 2^+ transitions are shown for the ^{6}Li+^{16}O doublets. The shape of the calculations differ noticeably from that of the data for the $2^+/1^-$ doublet, and so it appears that the 1^- state must be significantly excited in order to smooth the curve and improve the description.

The data and calculation for the scattering to the $5/2^-$, 2.43-MeV state in ^{9}Be are also shown in Fig. 16. In these data there is a precipitous dip at approximately $20^\circ_{\text{c.m.}}$ which the calculations do not reproduce completely, but the overall description is good. Measurements of this dip were repeated to confirm its depth. The value of

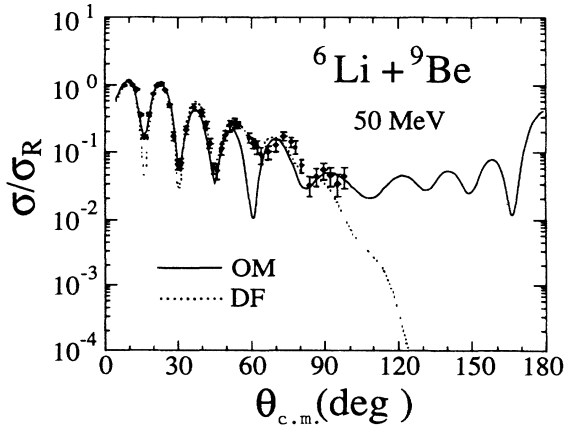

FIG. 15. Optical model (OM) and double folded (DF) description of 50-MeV ^{6}Li+^{9}Be elastic scattering.

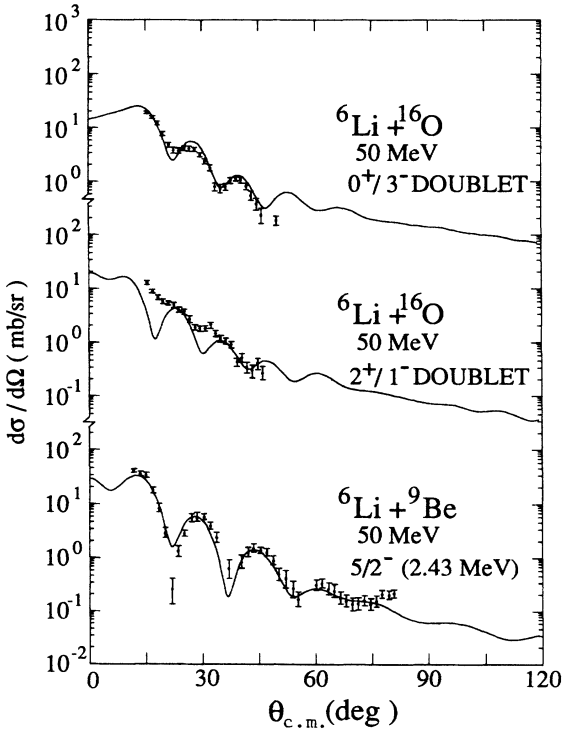

FIG. 16. Data and DWBA calculations for 50-MeV ^{6}Li scattering to the $0^+/3^-$ (6.05/6.13 MeV) doublet and $2^+/1^-$ (6.92/7.12 MeV) doublet in ^{16}O and to the $5/2^-$ (2.43 MeV) state in ^{9}Be.

TABLE III. ^{6}Li+^{9}Be 50-MeV potential parameters.

Potential	V (MeV)	N	r_R[a] (fm)	a_R (fm)	W (MeV)	r_I[a] (fm)	a_I (fm)
Ref. 14	174.0		1.22	0.75	5.84	2.81	0.63
Ref. 2	155.0		1.80	0.65	74.15[b]	1.80	0.65
OM	151.6		1.30	0.68	13.29	2.41	0.76
DF		0.51			17.27	2.14	0.79

[a]$R_x = r_x A_T^{1/3}$.
[b]Strength of a surface derivative imaginary potential.

βR_I of 1.60 fm compares with 1.70 fm previously determined for 32-MeV scattering.[14]

V. CONCLUSION

In summary, the 50-MeV ^{6}Li+^{12}C, ^{16}O, and ^{9}Be scattering experiments reported here have confirmed the existence of a plateau in the elastic scattering cross section in the mid-angle region (60°–100°) for scattering from ^{12}C and ^{16}O and have shown that this feature is not so apparent in the scattering from ^{9}Be. Further, the inelastic scattering from ^{12}C, ^{16}O, and ^{9}Be do not display such a plateau structure.

It has been demonstrated that by fitting the ^{6}Li+^{12}C elastic scattering data through the diffraction oscillations preceding the mid-angle plateau structure, it is possible to find a smooth energy dependence of the optical model parameters for ^{6}Li+^{12}C elastic scattering. These parameters have predictive power, for in the low- (11 and 20 MeV) and high- (156 and 210 Mev) energy regimes they are useful in describing the elastic scattering data throughout a wide angular range, and in the mid-energy regime (24, 30, 50, 60, and 99 MeV) they describe the data well through the first few diffraction oscillations preceding the plateau region. Further, it has been observed that when the energy-dependent potentials are used in DWBA calculations, an acceptable description of the inelastic scattering to the 2^+ (4.44 MeV) and 3^- (9.65 MeV) states in ^{12}C is given. Additionally, it has been shown that the inclusion of an angular momentum dependent absorptive potential can improve the description of ^{6}Li+^{12}C elastic scattering data and result in a description of 30-MeV ^{6}Li+^{12}C vector analyzing power data which is as good, or better, than that previously obtained. The double folding model description of the measured ^{12}C elastic scattering data is good in the low- and high-energy regimes. However, in the mid-energy region the double folding description does a poor job of describing the elastic scattering data. The analysis of the 50-MeV ^{6}Li+^{16}O and ^{9}Be scattering data has shown that the calculated elastic scattering angular distribution through the first diffraction oscillation is not sensitive to the specific shape of the Woods-Saxon optical potential and any reasonable Woods-Saxon potential can be used to check the normalization of data to ±20%; in the figures contained herein, this uncertainty is roughly equivalent to the size of a data point.

The authors gratefully acknowledge the support of this work by the National Science Foundation, the U.S. Department of Energy, and the State of Florida.

[1]A. Nadasen, M. McMaster, G. Gunderson, A. Judd, S. Villanueva, P. Schwandt, J. S. Winfield, J. van der Plicht, R. E. Warner, F. D. Becchetti, and J. W. Jänecke, Phys. Rev. C **37**, 132 (1988).
[2]J. E. Poling, E. Norbeck, and R. R. Carlson, Phys. Rev. C **13**, 648 (1976).
[3]M. F. Vineyard, J. Cook, and K. W. Kemper, Phys. Rev. C **31**, 879 (1985).
[4]H. G. Bingham, M. L. Halbert, D. C. Hensley, E. Newman, K. W. Kemper, and L. A. Charlton, Phys. Rev. C **11**, 1913 (1975).
[5]D. P. Stanley, F. Petrovich, and P. Schwandt, Phys. Rev. C **22**, 1357 (1980); P. Schwandt, W. W. Jacobs, M. D. Kaitchuck, P. P. Singh, W. D. Ploughe, F. D. Becchetti, and J. Jänecke, *ibid.* **24**, 1522 (1981).
[6]J. Cook, H. J. Gils, H. Rebel, Z. Majka, and H. Klewe-Nebenius, Nucl. Phys. **A388**, 173 (1982).
[7]M. F. Vineyard, J. Cook, K. W. Kemper, and M. N. Stephens, Phys. Rev. C **30**, 916 (1984).
[8]M. E. Brandan, S. H. Fricke, and K. W. McVoy, Phys. Rev. C **38**, 673 (1988).
[9]S. H. Fricke, M. E. Brandan, and K. W. McVoy, Phys. Rev. C **38**, 682 (1988).
[10]A. Bisson and R. H. Davis, Phys. Rev. Lett. **22**, 542 (1969).
[11]D. Robson, Proceedings of the Argonne Symposium on Heavy Ion Reactions (Argonne National Laboratory, Argonne, 1972), p. 239.
[12]L. T. Chua, F. D. Becchetti, J. Jänecke, and F. L. Milder, Nucl. Phys. **A273**, 243 (1976).
[13]W. Weiss, P. Egelhof, K. D. Hildenbrand, D. Kassen, M. Makowska-Rzeszutko, D. Fick, H. Ebinghaus, E. Steffens, A. Amakawa, and K.-I. Kubo, Phys. Lett. **61B**, 237 (1976).
[14]J. Cook and K. W. Kemper, Phys. Rev. C **31**, 1745 (1985).
[15]G. Bassani, N. Saunier, B. M. Traore, J. Raynal, A. Foti, and G. Pappalardo, Nucl. Phys. **A189**, 353 (1972).
[16]J. Cook, Comput. Phys. Commun. **31**, 363 (1984).

[17]J. Cook, At. Data Nucl. Data Tables **26**, 19 (1981).
[18]B. R. Fulton and T. M. Cormier, Phys. Lett. **97B**, 209 (1980).
[19]R. A. Chatwin, J. S. Eck, D. Robson, and A. Richter, Phys. Rev. C **1**, 795 (1970).
[20]J. S. Eck, R. A. LaSalle, and D. Robson, Phys. Rev. **186**, 1132 (1969).
[21]J. S. Eck, R. A. Chatwin, K. A. Eberhard, R. A. LaSalle, A. Richter, and D. Robson, *Nuclear Reactions Induced by Heavy Ions* (North-Holland, Amsterdam, 1970).
[22]S. P. Van Verst, D. P. Sanderson, D. E. Trcka, K. W. Kemper, V. Hnizdo, B. G. Schmidt, and K. R. Chapman, Phys. Rev. C **39**, 853 (1989).
[23]Y. Sakuragi, M. Yahiro, and M. Kamimura, Prog. Theor. Phys. Suppl. **89**, 136 (1986), and references therein.
[24]H. Nishioka, J. A. Tostevin, R. C. Johnson, and K.-I. Kubo, Nucl. Phys. **A415**, 230 (1984).
[25]G. R. Satchler and W. G. Love, Phys. Rep. **55**, 183 (1979).
[26]F. Petrovich, R. J. Philpott, A. W. Carpenter, and J. A. Carr, Nucl. Phys. **A425**, 609 (1984).
[27]G. Bertsch, J. Borysowicz, H. McManus, and W. G. Love, Nucl. Phys. **A284**, 399 (1977).
[28]F. Petrovich, H. McManus, V. A. Madsen, and J. Atkinson, Phys. Rev. Lett. **22**, 895 (1969).
[29]R. Schaefer, Nucl. Phys. **A158**, 321 (1970).
[30]G. R. Satchler and W. G. Love, Phys. Lett. **65B**, 415 (1976).
[31]L. R. Suelzle, M. Y. Yearian, and H. Crannell, Phys. Rev. **162**, 992 (1967).
[32]D. P. Stanley, Ph.D. thesis, Florida State University, 1979.
[33]P. D. Kunz (unpublished).
[34]K. Amos, W. Bauhoff, I. Morrison, S. F. Collins, R. S. Henderson, B. M. Spicer, G. G. Shute, V. C. Officer, D. W. Devins, D. L. Friesel, and W. P. Jones, Nucl. Phys. **A413**, 255 (1984).
[35]J. Cook, Nucl. Phys. **A445**, 350 (1985).
[36]G. E. Moore, K. W. Kemper, and L. A. Charlton, Phys. Rev. C **11**, 1099 (1975).
[37]R. M. DeVries, D. A. Goldberg, J. W. Watson, M. S. Zisman, and J. G. Cramer, Phys. Rev. Lett. **39**, 450 (1977).
[38]V. Hnizdo, K. W. Kemper, and J. Szymakowski, Phys. Rev. Lett. **46**, 590 (1981).